Climate Dynamics (2001) 18: 225–240

J. M. Gregory · J. A. Church · G. J. Boer
K. W. Dixon · G. M. Flato · D. R. Jackett
J. A. Lowe · S. P. O'Farrell · E. Roeckner
G. L. Russell · R. J. Stouffer · M. Winton

Comparison of results from several AOGCMs for global and regional sea-level change 1900–2100

Received: 1 September 2000 / Accepted: 20 April 2001

Abstract Sea-level rise is an important aspect of climate change because of its impact on society and ecosystems. Here we present an intercomparison of results from ten coupled atmosphere-ocean general circulation models (AOGCMs) for sea-level changes simulated for the twentieth century and projected to occur during the twenty first century in experiments following scenario IS92a for greenhouse gases and sulphate aerosols. The model results suggest that the rate of sea-level rise due to thermal expansion of sea water has increased during the twentieth century, but the small set of tide gauges with long records might not be adequate to detect this acceleration. The rate of sea-level rise due to thermal expansion continues to increase throughout the twenty first century, and the projected total is consequently larger than in the twentieth century; for 1990–2090 it amounts to 0.20–0.37 m. This wide range results from systematic uncertainty in modelling of climate change and of heat uptake by the ocean. The AOGCMs agree that sea-level rise is expected to be geographically non-uniform, with some regions experiencing as much as twice the global average, and others practically zero, but they do not agree about the geographical pattern. The lack of agreement indicates that we cannot currently have confidence in projections of local sea-level changes, and reveals a need for detailed analysis and intercomparison in order to understand and reduce the disagreements.

J. M. Gregory (✉) · J. A. Lowe
Hadley Centre, Meteorological Office,
London Road, Bracknell,
Berkshire RG12 2SY, UK
E-mail: jmgregory@meto.gov.uk

J. A. Church · D. R. Jackett
Antarctic CRC and CSIRO Marine Research,
Castray Esplanade, GPO Box 1538, Hobart,
Tasmania 7001, Australia

G. J. Boer · G. M. Flato
Canadian Centre for Climate Modeling and Analysis,
PO Box 1700, Victoria, British Columbia V8W 2Y2, Canada

K. W. Dixon · R. J. Stouffer · M. Winton
Geophysical Fluid Dynamics Laboratory,
PO Box 308, Princeton, New Jersey 08542, USA

S. P. O'Farrell
CSIRO Atmospheric Research, PMB 1,
Aspendale, Victoria 3195, Australia

E. Roeckner
Max-Planck-Institut für Meteorologie,
Bundestrasse 55, D-20146 Hamburg, Germany

G. L. Russell
NASA/Goddard Institute for Space Studies,
2880 Broadway, New York, New York 10025, USA

1 Introduction

Increases in the availability of computing power over the past few years have permitted time-dependent climate change experiments spanning two or more centuries to be carried out with coupled atmosphere-ocean general circulation models (AOGCMs). In order to assess the reliability of these models, and to address the question of whether anthropogenic climate change can be detected in the record of the past hundred years, climate change "hindcasts" from various AOGCMs have been compared with one another and with observations (Mitchell et al. 2001), focusing particularly on surface air temperature. Climate change predictions for the next hundred years using scenarios for future emissions or concentrations of greenhouse gases and aerosols have also been compared (Cubasch et al. 2001).

Sea-level rise is an important aspect of climate change because of its impact on society and ecosystems. During the twenty first century, global-average sea-level is expected to rise considerably faster than in the twentieth, with thermal expansion of seawater making the largest contribution. For instance, Warrick et al. (1996) give projections for sea-level rise 1990–2100 using two alternative climate models; from the models of Wigley and Raper (1993, 1995) the contributions to sea-level rise for 1990–2100 due to thermal expansion and land-ice melt

are 0.28 m and 0.21 m respectively, while from the model of De Wolde et al. (1997) they are 0.15 m and 0.12 m.

Sea-level would continue to rise due to thermal expansion for many centuries after atmospheric concentrations of greenhouse gases had been stabilised, because the deep ocean adjusts to climate change on a time scale of thousands of years (Manabe and Stouffer 1994; Stouffer and Manabe 1999; Weaver and Wiebe 1999; Knutti and Stocker 2000; Voss and Mikolajewicz 2001; Raper et al. 2001). The final level, therefore, could be considerably higher than that attained by 2100. For example, the final global-average sea-level rise due to thermal expansion in the model of Stouffer and Manabe (1999) is 1.96 m for a constant atmospheric CO_2 concentration of twice its initial value.

AOGCM results can be used to calculate global-average sea-level rise due to thermal expansion and the geographical distribution of sea-level change resulting from changes in ocean density and circulation (Gregory 1993; Cubasch et al. 1994; Bryan 1996; Jackett et al. 2000; Russell et al. 2000a; Gregory and Lowe 2000). However, fewer results have been published for sea-level rise from AOGCMs than for temperature and other aspects of climate change. Furthermore, up to now there has been no systematic intercomparison of results obtained from different models. To address this need, we present and compare the results here from several AOGCMs run with the same scenario for past and future atmospheric composition. We assess the systematic uncertainty in the predictions and comment on the comparison with recent observed sea-level changes.

2 Models and scenario

The models included in this analysis and the centres where they were developed are shown in Table 1. With each model, two parallel climate experiments were run: control and "GS". The control integrations have a constant atmospheric composition, reflecting conditions prior to the twentieth century. Each GS integration begins from a state chosen from its control, taken to represent the latter part of the nineteenth or early twentieth century, a time sufficiently long before the present that the "cold start" effect (Hasselmann et al. 1993; Keen and Murphy 1997) is essentially eliminated. The atmospheric concentrations of greenhouse gases and sulphate aerosols increase according to historical observations up to 1990. After 1990, the GS integrations follow scenario IS92a (Leggett et al. 1992), which assumes mid-range economic growth but no measures to reduce greenhouse-gas emissions. (Most AOGCMs have not yet been run with more recently developed scenarios.)

The change in sea-level due to climate change is defined as the difference between sea-level in the GS and the control integrations. Careful consideration is needed of which control state should be subtracted. The control run is intended to simulate a constant climate and should therefore have no trend in sea-level. However, if the model has not been spun up to a steady state before the beginning of the experiment, it may exhibit some drift. In the control run of a typical AOGCM there is more likely to be a drift in sea-level than in any parameter of the surface climate because sea-level approaches a steady state on the long time scales associated with the deep ocean, whereas the surface climate has comparatively little thermal inertia and equilibrates with the forcing on the time scale of about a decade.

For CGCM1, CGCM2, CSIRO Mk2, ECHAM4/OPYC3 and GISS2, any control drift is eliminated by evaluating the sea-level change as the difference between corresponding times in the GS and control runs, on the assumption that the drift is combined linearly with the climate change signal in the GS run. In this method, the temporal variability of sea-level in the control run will affect the results for sea-level change. With the GFDL and Hadley Centre models, methods were used which suppress the effect of control variability in the sea-level change fields. For GFDL_R15_b and GFDL_R30_c, there was negligible drift, so a long-term mean from the control was subtracted from the GS fields. For HadCM2 and HadCM3, a cubic function of time was fitted at each point to the decadal time series of local sea-level from the control run; fields calculated from the fit, rather than the original control fields, were subtracted from the corresponding decades in GS run. This procedure removes the drift while eliminating the variability from the control.

The results quoted for GFDL_R15_b are from an average of an ensemble of six parallel GS integrations, starting from slightly different initial conditions. These integrations rapidly diverge in detail within the envelope of internal variability; the ensemble mean gives a statistically more accurate estimate of the climate change. Ensembles of integrations have been carried out for some other models too, but the results quoted here depend on only one GS integration in cases other than GFDL_R15_b.

The fields of sea-level change are the data on which the analysis in the rest of this study is based. We do not look at the GS or control integrations separately. At some points, we have to make statistical adjustments to take into account the different ways in which sea-level change was evaluated in the various models.

In ECHAM4/OPYC3 and HadCM3, individual trace gases are separately specified; in the other models, all greenhouse gases are represented by a "equivalent" concentration of CO_2 giving the same radiative forcing of the climate system. In all the models except CSIRO Mk2, ECHAM4/OPYC3, GISS2 and HadCM3, equivalent CO_2 rises at 1% per year compounded after 1990. This is an approximation to IS92a which gives an overestimate of the radiative forcing compared with IS92a, by 15% at 2100 (Mitchell et al. 2000). HadCM3 and GISS2 calculate the direct effect of sulfate aerosol (the reflection of sunlight by aerosol particles) in their radiation schemes, but the other models represent it by increasing the surface albedo. HadCM3 also includes an estimate of the indirect effect of sulfate aerosols (reducing cloud water droplet size and hence increasing cloud albedo and lifetime) and changes in tropospheric ozone. Since the sum of these effects tends to cool the climate system, HadCM3 experiences a smaller radiative forcing than the other models. Despite these differences, the experiments are roughly comparable as regards radiative forcing, so their differences result mainly from model formulation.

The GISS2 GS integration used a CO_2 increase of 0.5% per year compounded, rather than 1%. Since this is substantially different from IS92a, we do not consider the time-development of the GISS integration. We include it only in the comparison of the geographical patterns of change (Sect. 4.3).

The ocean components of the AOGCMs have a range of resolutions, between 1° and 6° in the horizontal and 11 and 29 unequally spaced vertical levels (Table 1). Except for GISS2 and OPYC3 (the ocean component of ECHAM4/OPYC3), all the ocean models are "rigid-lid" models with depth z as the vertical coordinate, in which the ocean has a fixed volume and a flat surface at $z = 0$. In these models, sea-level change has to be deduced indirectly, as described in the following sections and the Appendix. GISS2 and OPYC3 have a free ocean surface.

3 Global-average sea-level rise due to thermal expansion

In rigid-lid models, global-average sea-level rise due to thermal expansion is estimated from density changes. Assuming that mass is conserved, the global-average sea-level rise is

Table 1 Climate models used in the analysis

Model	Ocean resolution long × lat × levels	Data available	Centre	References
CGCM1	1.8° × 1.8° × 29	1900–2100	CCCma	Flato et al. (2000), Boer et al. (2000a, b)
CGCM2	1.8° × 1.8° × 29	1901–2100	CCCma	Flato and Boer (2001)
CSIRO Mk2	5.6° × 3.2° × 21	1881–2100	CSIRO	Gordon and O'Farrell (1997), Hirst et al. (2000)
ECHAM4/OPYC3	2.8° × 2.8°[a] × 11	1860–2049	DKRZ	Roeckner et al. (1996, 1999)
GFDL_R15_a	3.7° × 4.5° × 12	1766–2065	GFDL	Manabe et al. (1991), Haywood et al. (1997)
GFDL_R15_b	3.7° × 4.5° × 12	1766–2095	GFDL	Dixon and Lanzante (1999)
GFDL_R30_c	1.875° × 2.25° × 18	1866–2090	GFDL	
GISS2	5.0° × 4.0° × 13	1950–2100	GISS	Russell et al. (2000a, b)
HadCM2	3.75° × 2.5° × 20	1860–2100	UKMO	Johns et al. (1997), Mitchell et al. (1995)
HadCM3	1.25° × 1.25° × 20	1860–2100	UKMO	Gordon et al. (2000), Johns et al. (2001)

[a] This model has increased latitudinal resolution near the Equator. The modelling centres are the Canadian Centre for Climate Modeling and Analysis (CCCma) in Victoria, the Division of Atmospheric Research of the Commonwealth Scientific and Industrial Research Organisation (CSIRO) in Melbourne, the German Climate Research Centre (DKRZ) in Hamburg, the Geophysical Fluid Dynamics Laboratory (GFDL) in Princeton, the NASA/Goddard Institute for Space Studies (GISS) in New York, and the Hadley Centre for Climate Prediction and Research of the Met Office in Bracknell (UKMO)

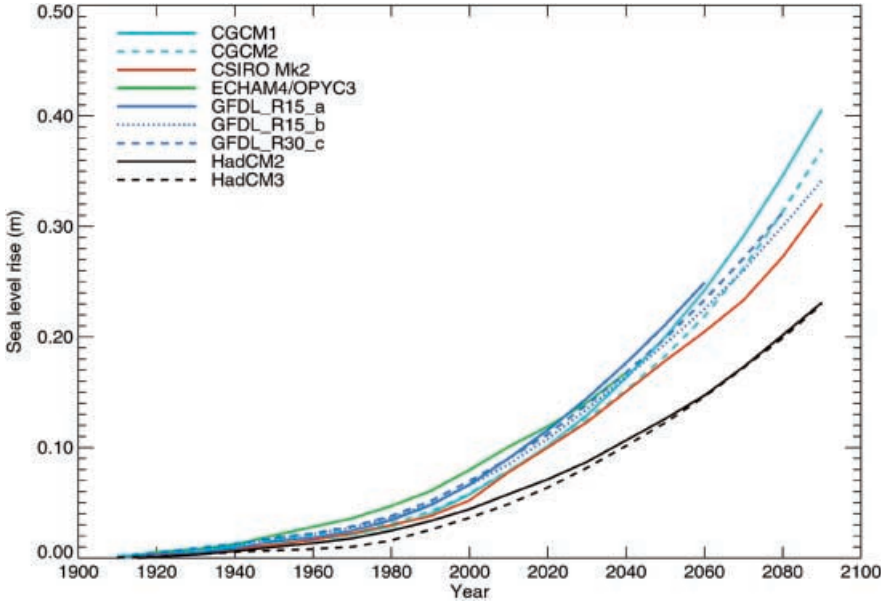

Fig. 1 Global-average sea-level rise due to thermal expansion. The curves have been offset on the *y*-axis so that they all have a mean of zero for 1910

$$r = -\frac{1}{S}\int_{S}\int_{-H}^{0}\frac{\Delta\rho}{\rho}\,\mathrm{d}z\,\mathrm{d}S\ , \qquad (1)$$

where z is positive upwards, S is the surface area of the ocean, H the depth as a function of location, and ρ the in-situ density. Changes in density due to changes in salinity make a negligible contribution to global-average sea-level rise, provided the global integral of salinity is conserved (Gregory and Lowe 2000). (Sea-level changes in individual oceans or smaller regions, however, can be substantially affected by salinity.)

Global-average sea-level rise from thermal expansion as a function of time is shown in Fig. 1 for each of the models and the average rate for various intervals in Table 1. The time series were plotted from decadal means, and it is notable that they are rather smooth. Time series of decadal-mean global-average surface air temperature show considerably more variability, but since sea-level reflects the heat content of the entire volume of the ocean, much of the surface variability is smoothed out by the integrating effect of the intermediate and deep layers.

Averaged over the period 1910–1990, the models give rates of sea-level rise lying in the range 0.3–0.8 mm a^{-1}, while for 1955–1995 they give 0.6–1.0 mm a^{-1}. For the latter period, an estimate of 0.55 mm a^{-1} (J. I. Antonov, personal communication), at the low end of the model range, has been obtained by the analysis of observations of interior ocean temperature changes (Levitus et al. 2000).

Over the following hundred years 1990–2090 the average model rates are within the range 2.0–3.7 mm a^{-1}. The increase compared with the twentieth century is consistent with the faster rate of climate change expected for the twenty first century. The global-average surface

air temperature change between 1990 and 2090 is between 2.6 and 3.9 °C in these integrations (Table 2), which should be compared with the temperature change of ~ 0.6 °C that has occurred in the last hundred years.

Upon differentiating with respect to time to obtain the rate of sea-level rise due to thermal expansion (Fig. 2), each of the models shows a steady acceleration during the twenty first century, with values ranging between 0.021 and 0.048 mm a^{-1} i.e. 2.1–4.8 mm a^{-1} per century (Table 2). A constant acceleration implies that thermal expansion increases quadratically with time during the twenty first century.

Global-average sea-level rise r due to thermal expansion is nearly proportional to the total amount of heat absorbed by the oceans. The cofficient of proportionality is called the "expansion efficiency of heat" by Russell et al. (2000a) and is model-dependent, according to whether the heat is absorbed into warmer or colder waters. Because of the proportionality, the steadily increasing rate of sea-level rise implies that the net heat flux F into the ocean is increasing steadily. In these integrations, the global-average surface air temperature change ΔT also increases roughly linearly in time during the twenty first century. Correlations between dr/dt ($\propto F$) and ΔT for the GS experiments have coefficients of 0.9 or above except for CSIRO Mk2 (0.83) and ECHAM4/OPYC3 (0.63). Combining these points suggests that $F \propto \Delta T$ during climate change with steadily increasing forcing (Gregory and Mitchell 1997). (This relation will fail for constant radiative forcing, when the system will approach a steady state, with $\Delta T \rightarrow$ constant and $F \rightarrow 0$.)

There are various distinct physical processes responsible for ocean heat uptake operating in different regions of the world. Moreover, surface air temperature change is not the only relevant climate parameter; salinity and wind stress changes are also important, for instance. The existence of a relation between F and ΔT implies only that changes in heat uptake processes can be scaled against global-average surface air temperature change taken as a single indicator of the magnitude of climate change. It remains to find physical explanations for the relation (see also Gregory 2000).

Despite being projections for the same scenario, the model results for sea-level rise during the twenty first century span a large range, approaching a factor of two between the largest and the smallest. This range reflects systematic uncertainty in modelling of both climate change in response to radiative forcing (the main influence on ΔT) and the relationship between climate change and heat uptake ($F \propto \Delta T$) (Cubasch et al. 2001; Church et al. 2001). Differences among models regarding their sensitivity to radiative forcing have already been the subject of much study (e.g. Cubasch et al. 2001), though the uncertainties remain large. Detailed intercomparison of AOGCM ocean heat uptake mechanisms has not yet been undertaken.

4 Local sea-level variability and change

4.1 Methods of calculation

Local sea-level is dynamically determined by ocean circulation and atmospheric pressure. Changes in ocean circulation are a consequence of changes both in three-dimensional density structure and in surface windstress forcing. Sea-level can be diagnosed directly in GISS2 and OPYC3. In the rigid-lid models, the pressure exerted on the water column by the horizontal rigid lid can be used as a proxy for local sea-surface height.

Four different methods, detailed in the Appendix, have been used in the different rigid-lid models for obtaining changes in the rigid-lid pressure and hence in local sea-level. Two of these methods make no assumptions about the nature of the ocean circulation, one

Table 2 Changes in global average sea-level and temperature during the twentieth and twenty first centuries. The figures for rate of sea-level rise are averages over the periods indicated. ΔT is the change in global average surface air temperature between 1990 and 2090. The figures for accelerations were obtained by linear regression of the rate of rise against time over the periods indicated

Model	Rate of rise/mm a^{-1}				ΔT/°C 1990–2090	Acceleration/10^{-2} mm a^{-2}		
	1910–1990		1990–2040	1990–2090		1910–1990		1990–2100
	Full	Nine				Full	Nine	
CGCM1	0.48	0.33	2.5	3.7	3.9	0.7 ± 0.2	0.0 ± 1.3	4.8 ± 0.2
CGCM2	0.50	0.27	2.2	3.3	3.6	0.5 ± 0.3	0.2 ± 1.1	4.4 ± 0.4
CSIRO Mk2	0.47	0.42	2.3	2.8	2.7	1.1 ± 0.2	2.0 ± 0.5	2.8 ± 0.7
ECHAM4/OPYC3	0.75	0.73	2.1			1.0 ± 0.5	2.9 ± 1.1	2.3 ± 0.9
GFDL_R15_a	0.59		2.6			1.5 ± 0.4		3.0 ± 0.1
GFDL_R15_b	0.60	0.68	2.3	2.9	3.2	1.1 ± 0.3	1.7 ± 1.4	2.6 ± 0.1
GFDL_R30_c	0.64	0.69	2.3	3.0	2.8	1.2 ± 0.3	1.7 ± 1.0	2.8 ± 0.1
HadCM2	0.42	0.43	1.5	2.0	2.6	0.9 ± 0.2	1.5 ± 1.3	2.1 ± 0.2
HadCM3	0.32	0.30	1.5	2.0	2.8	1.3 ± 0.4	1.3 ± 1.2	2.2 ± 0.2

The columns marked "Nine" were computed from nine gridboxes, representing the regions of Douglas (1997); the uncertainty on the "Nine" acceleration was adjusted to take into account the cases where a difference or an ensemble was used to evaluate the fields of sea-level change (see also Sect. 5.2). All other columns were computed from the full fields

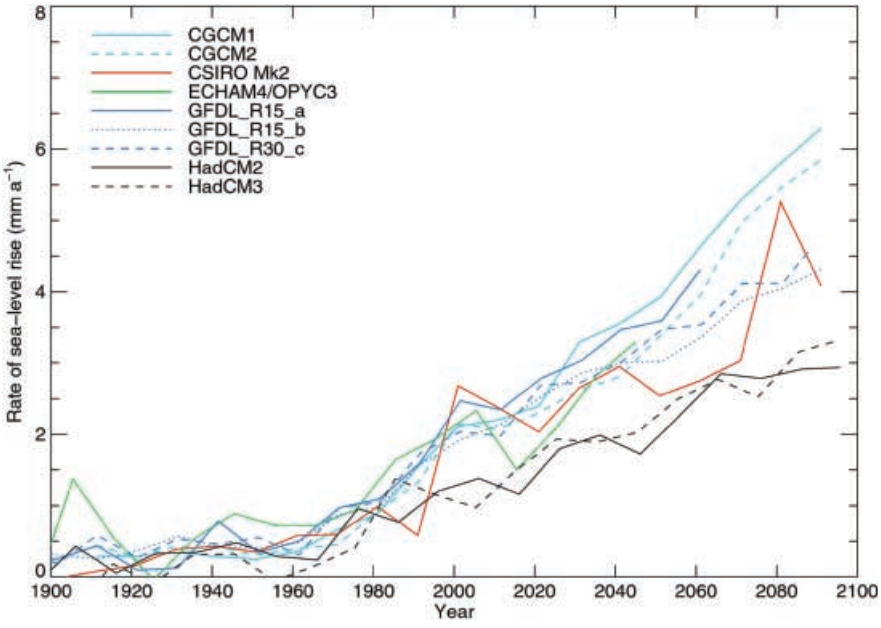

Fig. 2 Rate of global-average sea-level rise due to thermal expansion

assumes geostrophy, and the last is the traditional oceanographic method assuming both geostrophy and a level of no motion. Despite their different bases, the methods produce very similar results when applied to the same dataset.

Changes in atmospheric pressure alter the sea-level through the "inverted barometer" effect; when air pressure falls, sea-level rises. Since water is practically incompressible, there is no inverted barometer effect on global-average sea-level. For long time scales, the expected relation is that a pressure fall of 1 mbar (100 Pa) is accompanied by a sea-level rise of about 1 cm. Deviations from this relation due to wind-forcing and resonant responses may be important on subannual time scales (Trupin and Wahr 1990; Ponte and Gaspar 1999), and due to restriction on flow through narrow channels into isolated basins (Ducet et al. 1999). In simulations of the twenty first century climate, changes in local mean sea-level atmospheric pressure do not exceed a few mbar. While not negligible, the consequent changes of a few cm in sea-level are small compared with the effects of changes in ocean circulation. Therefore the inverted barometer effect is not included in any of the results we present.

Because the ECHAM4/OPYC3 GS integration ends at 2050, for analysis of local sea-level change we make use of an ECHAM4/OPYC3 integration with greenhouse gases only i.e. no sulfate aerosol. We assume that the geographical pattern will be substantially unaffected by the somewhat different radiative forcing. This is supported by comparing corresponding decades from the GS and greenhouse-gas-only integrations of other AOGCMs; in all available cases the spatial correlation coefficients exceed 0.8 in the latter decades of the twenty first century.

Note that GFDL_R15_a is omitted from this section because fields were not available for analysis of local sea-level changes.

4.2 Spatial variance of sea-level

A common conclusion from all the models is that sea-level change is far from uniform (Fig. 3). The non-uniformity can be quantified by evaluating the area-weighted standard deviation of the fields. Suppose that local sea-level change h can be written as a function of location $\mathbf{x}$ and time t:

$$h(\mathbf{x}, t) = R(\mathbf{x}, t) + \epsilon(\mathbf{x}, t) \ , \qquad (2)$$

i.e. local sea-level change consists of a pattern R associated with climate change, on which is superimposed the local variability ϵ, having zero time average. In the absence of climate change (and if there is no model drift), R is zero at all locations and all times, while ϵ is the local variability of sea-level. In an ensemble of simulations of future climate change (starting from slightly different initial conditions so that they diverge in detail), R would be the same in all the simulations, but ϵ would be different in each one. In the mean over ensemble members, ϵ would tend to average out. R might be a time-invariant geographical pattern with a time-dependent amplitude (i.e. the product of a function of space only with a function of time only), but we are not assuming that this is the case. Because changes in different regions of the ocean are affected by different processes, they do not all take place at the same rate; hence the pattern of sea-level change as well as the amplitude may evolve as time passes.

At any given time, the spatial variance of h will be

$$\sigma_h^2(t) = \sigma_R^2(t) + \sigma_\epsilon^2(t) \ , \qquad (3)$$

assuming that R and ϵ are not spatially correlated. (Each spatial variance is the area-weighted integral of the deviation from the area-weighted mean, and is written as the square of a spatial standard deviation.) From the

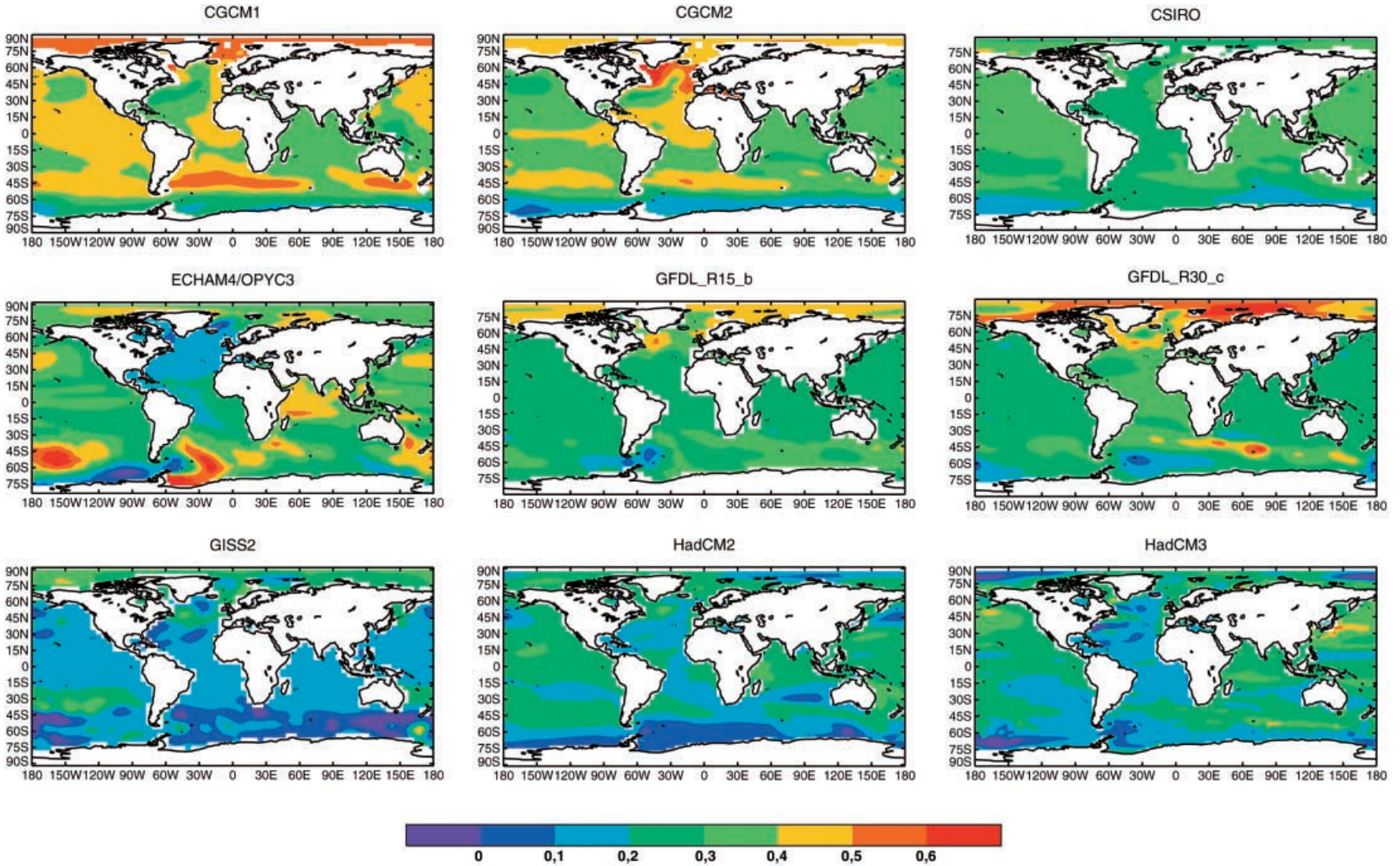

Fig. 3 Sea-level change over the twenty first century. Each field is the difference in sea-level between the last decade of the experiment and the decade 100 years earlier. The contour interval is 0.1 m

AOGCM results, we find that the spatial standard deviation of sea-level change (σ_h) increases in time for all models (Fig. 4), reaching 0.05–0.12 m by the end of the twenty first century, roughly 15–30% of the global average (Fig. 1, Table 3). ECHAM4/OPYC3 has a much higher spatial variability than the other models (Fig. 4). The increase in σ_h with time is consistent with our expectation that the spatial standard deviation associated with climate change (σ_R) will grow as the local sea-level response to climate change becomes more pronounced i.e. as the climate-change signal emerges above the noise.

During most of the twentieth century, σ_h is relatively small and increases rather little. Equation 3 suggests that this could be because σ_R is small compared with the the spatial standard deviation of sea-level resulting from variability (σ_ϵ) i.e. the signal of sea-level change cannot be distinguished from the background of noise in any one decade.

We can back this up by making an estimate of the size of the variability. We fit a separate quadratic function of time at each point to the timeseries of local sea-level change in the twenty first century, and take $\epsilon(\mathbf{x}, t)$ to be the residual field for the decade at time t. The spatial variance due to temporal variability (σ_ϵ^2) is evaluated as the time-average spatial variance of these residual fields. (This assumes that the characteristics of variability do not change with time.) If a quadratic fit is inadequate, the size of ϵ will be overestimated, but we find that a cubic cannot be successfully fitted at many points because the quadratic residuals do not have any tendency consistent with higher-order polynomials. We judge that a linear fit is inadequate, because it is rejected at more points than expected by chance in a test on χ^2 calculated with the residual variance from the quadratic fit in the denominator.

Estimated by the above means, σ_ϵ is about the same size as the spatial standard deviation of sea-level (σ_h) early in the twentieth century (Fig. 4, Table 4). In cases where the sea-level change fields were obtained as a difference between decadal means from two independent integrations, our estimate of σ_ϵ^2 has to be divided by 2 to obtain an estimate of local decadal variability in either run individually. For GFDL_R15_b, which used an average of six runs, σ_ϵ^2 has to be multiplied by 6. Since temporal variability in sea-level on decadal time scales is not strongly correlated over the majority of the world, the adjusted spatial standard deviation σ_ϵ^* can be taken as an indication of the amplitude of local decadal sea-level variability. It lies in the range 0.01–0.02 m (except for ECHAM4/OPYC3, which has 0.03 m).

4.3 Geographical pattern of sea-level change during the twenty first century

We remarked that the pattern as well as the magnitude of sea-level change might evolve with time. However, it turns out that for each model the geographical pattern of sea-level change is fairly stable through the latter half of the twenty first century, as we can show by calculating the area-weighted correlation coefficients between the field of sea-level change from the final decade of the experiment and all the earlier fields (Fig. 5). (Note that the correlation is the usual centred coefficient, which is unaffected by differences in the global average; it measures only the similarity of the geographical patterns.) The correlation increases with time, passing 0.8 by about 2050 in all cases. This also confirms that the growth in σ_R outweighs any increase in the variability σ_ϵ, because variability can only reduce the correlation. We take the last available decade of the twenty first century as representative of the pattern (Fig. 3). For that decade, model results show some locations with sea-level rise of more than twice the global average, and others with a sea-level fall (Table 3).

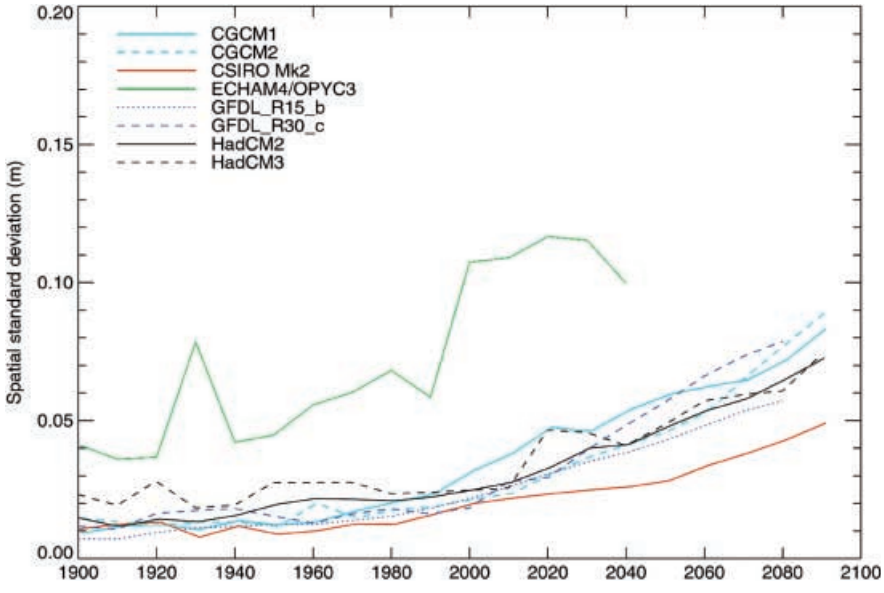

Fig. 4 Spatial standard deviation of local sea-level change with respect to the control climate

Although the pattern from any one model is fairly constant, the patterns given by the different models are not similar in detail and correlations between them are generally low (Table 5). The largest correlations are between pairs of models which are very similar in formulation viz 0.65 between CGCM1 and CGCM2, 0.63 between GFDL_R15_b and GFDL_R30_c. The greatest correlations between models from different centres are 0.60 between CSIRO Mk2 and HadCM2 and 0.58 between CGCM2 and GFDL_R30_c, and there are five others in the range 0.4–0.5. Since we do not have available the control sea-level fields from all the models, a detailed analysis of the significance of the results is not possible. However, as an indication, we note that 95% of the correlation coefficients between all different pairs of 24 decadal mean sea-level fields from the HadCM2 control run, with the long-term mean subtracted, lie within −0.4 and +0.4. Assuming that this is typical of uncorrelated variability, correlation coefficients with absolute values greater than ~ 0.4 probably indicate significant similarity.

Inspection of the sea-level fields (Fig. 3) reveals few common features. To obtain a quantitative assessment of the significance of large-scale patterns, we divide the ocean into 12 regions and for each model we test whether the regional-average sea-level change over the twenty first century is significantly different from the global average sea-level change. To do this, we obtain an estimate of the decadal variability in the difference between regional and global averages by fitting a quadratic to the time series of differences in the twenty first century, similar to the method used for ϵ. We then evaluate the hypothesis that the difference between global and regional sea-level change over the twenty first century is consistent with zero, using a two-tailed t-test at a significance level of 5%. Most regional changes are found to be significantly different from the global average (Table 6), but there are only two regions where there is a clear majority of models in agreement over the sign of the difference.

Seven of the eight models exhibit a larger than average sea-level change in the Arctic Ocean (and none show a minimum). As suggested by Bryan (1996), this feature could be caused by a freshening due to increased river inflow or precipitation; reduced salinity leads to reduced density and a compensating local sea-level rise (see Miller and Russell 2000).

Six of the eight models show a minimum of sea-level change in the Southern Ocean (and none show a maximum), as also found by Manabe et al. (1991), Gregory (1993), Bryan (1996) and Jackett et al. (2000). The Southern Ocean is a region of pronounced heat uptake (e.g. Murphy and Mitchell 1995; Hirst et al. 1996; Gregory 2000), but thermal expansivity is small at the cold water temperatures of high southern latitudes and some of the heat is exported to lower latitudes. Changes in wind stress may also affect the sea-level drop across the Antarctic Circumpolar Current.

Bryan (1996) drew attention to a dipole pattern of sea-level change in the northwest Atlantic, which is also seen in all the models considered here except ECHAM4/OPYC3. In the longitudes 40–50°W, for instance, sea-level rise is enhanced to the north and reduced to the south of the approximate latitude of the North Atlantic Drift (Fig. 6). Insofar as this current is a branch of the North Atlantic overturning circulation, the sea-level pattern is consistent with the weakening observed in

Table 3 Area-weighted standard deviation and the minimum and maximum values, divided by the area-weighted average, for sea-level change during the twenty first century. The sea-level change was calculated by finding the difference between the final decade of each experiment (see Table 1) and the decade 100 years earlier

Model	SD	Minimum	Maximum
CGCM1	0.19	0.3	1.6
CGCM2	0.23	0.2	2.2
CSIRO Mk2	0.15	0.5	1.3
ECHAM4/OPYC3	0.34	−1.2	2.3
GFDL_R15_b	0.18	0.3	1.8
GFDL_R30_c	0.25	0.2	2.5
GISS2	0.48	−1.5	3.1
HadCM2	0.29	−0.1	1.7
HadCM3	0.32	−0.5	2.2

Table 4 Spatial and temporal variance of sea-level

Model	σ_ϵ/m	σ_M/mm a^{-1}	σ^*_ϵ/m	σ^*_M/mm a^{-1}	V^*/σ^{*2}_M	σ_9/mm a^{-1}
CGCM1	0.009	0.22	0.006	0.20	0.24	0.33
CGCM2	0.009	0.20	0.006	0.17	0.32	0.23
CSIRO Mk2	0.010	0.20	0.007	0.18	0.33	0.18
ECHAM4/OPYC3	0.035	0.64	0.025	0.48	0.75	0.27
GFDL_R15_b	0.004	0.16	0.010	0.21	0.51	0.13
GFDL_R30_c	0.010	0.24	0.010	0.24	0.38	0.16
HadCM2	0.011	0.37	0.011	0.37	0.24	0.25
HadCM3	0.017	0.47	0.017	0.47	0.40	0.38

σ_ϵ is the spatial standard deviation of temporal variability deduced from decadal-mean fields of sea-level change. σ^*_ϵ is the same quantity adjusted to take into account the cases where a difference or an ensemble was used to evaluate the fields of sea-level change; this quantity is an estimate of the decadal-mean temporal standard deviation of sea-level. σ_M is the spatial standard deviation of estimated trends of local sea-level rise during 1910–1990. σ^*_M is the same quantity adjusted as for σ^*_ϵ. The ratio V^*/σ^{*2}_M is the proportion of spatial variance of trends explained by temporal variability V. σ_9 is the spatial standard deviation of trends during 1910–1990 from a set of nine gridboxes distributed following Douglas (1997)

most AOGCM experiments. In ECHAM4/OPYC3, the Atlantic overturning circulation does not weaken (Latif et al. 2000), consistent with the absence of this pattern.

5 Sea-level change in the twentieth century

5.1 Spatial variance of sea-level trends

As we saw in Sect. 4, the geographical pattern of sea-level change in any single decade of the twentieth century by itself cannot be distinguished from variability, since the signal-to-noise ratio is too low. However, it may be possible to discern the geographical non-uniformity in local trends over several decades taken together, because using a longer period will reduce the influence of temporal variability. In practice, local sea-level trends are obtained by linear regression against time of tide-gauge records, which provide the only observational time series that extend over many decades. (Although satellite altimetry is a promising technique for the future, it has so far provided less than a decade of continuous measurements.) Observations show no evidence of acceleration (a point we return to at the end of this section), and we use a linear fit in our analysis for consistency with this. Nonetheless, we expect (Table 2) an acceleration in sea-level rise due to thermal expansion in the twentieth century, unless this acceleration is offset by some other term, such as one of those discussed later (Sect. 5.2).

Suppose that $T(\mathbf{x})$ is the slope of the best linear fit of $R(\mathbf{x},t)$ (sea-level change due to climate change) against time. Because of the presence of variability ϵ (see Eq. 2), the best linear fit to local sea-level change $h(\mathbf{x},t)$ will have a slope $M(\mathbf{x})$ that differs from $T(\mathbf{x})$ in general. The geographical variation of ϵ will inflate the spatial variance σ_M^2. Let us write

$$\sigma_M^2 = \sigma_T^2 + V \ ,$$

where σ_T^2 is the spatial variance due to the geographical dependence of R, and V is the additional variance due to variability. (This equation is the analogue for sea-level trends of Eq. 3.)

Using the AOGCM data, we can estimate V, following a bootstrap method. First, we find the spatial variance of fitted local trends 1910–1990. Then to the

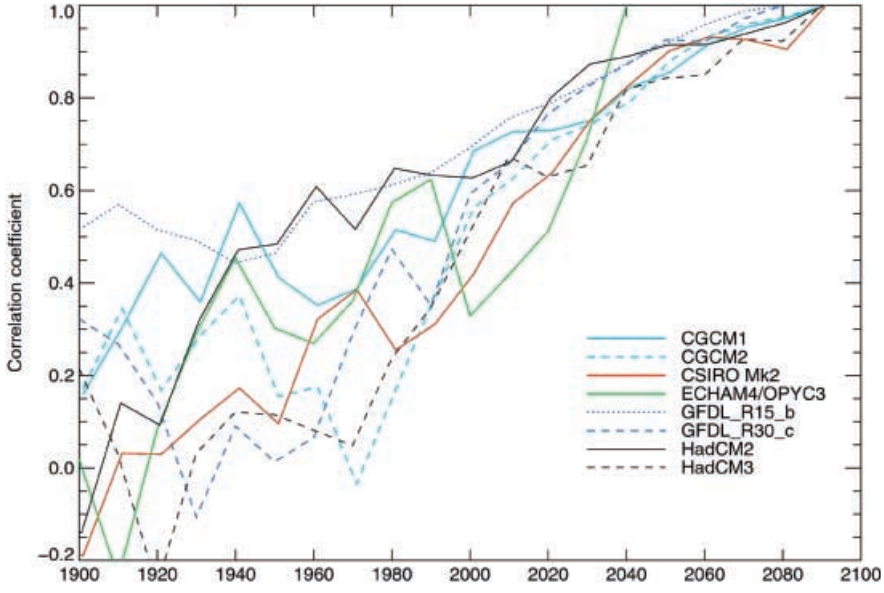

Fig. 5 Correlation of the pattern of sea-level change at the end of the twenty first century with earlier decades

Table 5 Area-weighted correlation coefficients between geographical patterns of sea-level change during the twenty first century from pairs of models

	1	2	3	4	5	6	7	8	9
1 CGCM1	1.00								
2 CGCM2	0.65	1.00							
3 CSIRO Mk2	0.45	0.37	1.00						
4 ECHAM4/OPYC3	0.09	−0.14	0.29	1.00					
5 GFDL_R15_b	0.21	0.28	−0.02	0.12	1.00				
6 GFDL_R30_c	0.45	0.58	0.05	−0.15	0.63	1.00			
7 GISS2	0.10	0.25	0.22	−0.16	0.00	0.10	1.00		
8 HadCM2	0.41	0.50	0.60	0.19	0.08	0.20	0.30	1.00	
9 HadCM3	0.25	0.09	0.47	0.34	0.13	0.07	0.03	0.37	1.00

The fields were averaged onto a common 5°-grid before the correlations were computed

linearly fitted twentieth-century fields we add randomly chosen twenty-first-century ϵ fields from the same AOGCM, fit linear trends again, and calculate the new spatial variance. (The ϵ fields are the residuals from the quadratic fit for the twenty first century.) The increase in spatial variance is taken as an estimate of V. We repeat the procedure 100 times, and find the average V. The spatial standard deviation of trends σ_M^* lies between 0.18 and 0.48 mm a^{-1} (Table 4). (The asterisk denotes adjustment for differences and ensembles of runs, as was done earlier for σ_ϵ.) The proportion V^*/σ_M^{*2} of the spatial variance explained by variability ranges from about 25% to about 50%, with ECHAM4/OPYC3 being an outlier at 75%. Although the importance of variability differs greatly between models, it thus appears that σ_T^2 is larger than V^* in most cases, i.e. in most models, a larger part of the spatial variance of simulated twentieth-century sea-level trends is due to climate change than to temporal variability. This suggests the possibility that there may be a statistically significant geographical pattern due to climate change in the twentieth-century sea-level trends.

Table 6 Significant regional sea-level changes. The table shows the number of models with significantly less or significantly more than global average sea-level rise in the various regions during the twenty first century. There are eight models in total

Region	Less	More
Arctic Ocean (north of 67°N in the Atlantic)	0	7
Atlantic Ocean 30°N–67°N	3	3
Atlantic Ocean 30°S–30°N	5	2
Indian Ocean north of Equator	4	4
Indian Ocean 30°S–0°	3	4
Mediterranean Sea	5	3
Pacific Ocean north of 30°N	2	2
Pacific Ocean 30°S–30°N west of 180°	3	3
Pacific Ocean 30°S–30°N east of 180°	4	3
Pacific Ocean 60°S–30°S	1	4
Atlantic and Indian Oceans 60°S–30°S	3	4
Southern Ocean south of 60°S	6	0

5.2 Comparison with estimates based on tide gauges

The model estimates for thermal expansion in the twentieth century (Table 2) are substantially smaller than the observational estimate of 1.0–2.0 mm a^{-1} of sea-level rise based on tide-gauge records (Church et al. 2001). This is because of contributions from factors other than thermal expansion. The widespread recession of glaciers has resulted in an increase of mass of the world ocean (Meier 1984; Zuo and Oerlemans 1997). There may also have been significant contributions to ocean mass from the Antarctic and Greenland ice-sheets (though the sign of these terms is uncertain) (Church et al. 2001), extraction of groundwater which subsequently finds its way to the sea (a positive term) (Gornitz et al. 1997; Sahagian 2000), and impoundment of water in reservoirs (a negative term) (Gornitz et al. 1997; Sahagian 2000). Addition or subtraction of water will not have altered sea-level uniformly, because of changes to the geoid caused by redistribution of mass from land to ocean, and changes in loading on the crust by ice and ocean (Nakiboglu and Lambeck 1991; Mitrovica et al. 2001). These effects are not simulated by the AOGCMs, and are in addition to the non-uniformity due to changes in ocean circulation and density.

Measurements of local sea-level change by tide gauges are affected by movement of the land on which the gauges are sited, in particular due to post-glacial isostatic adjustment, which in some regions is comparable to or larger than the effect of ocean changes; see

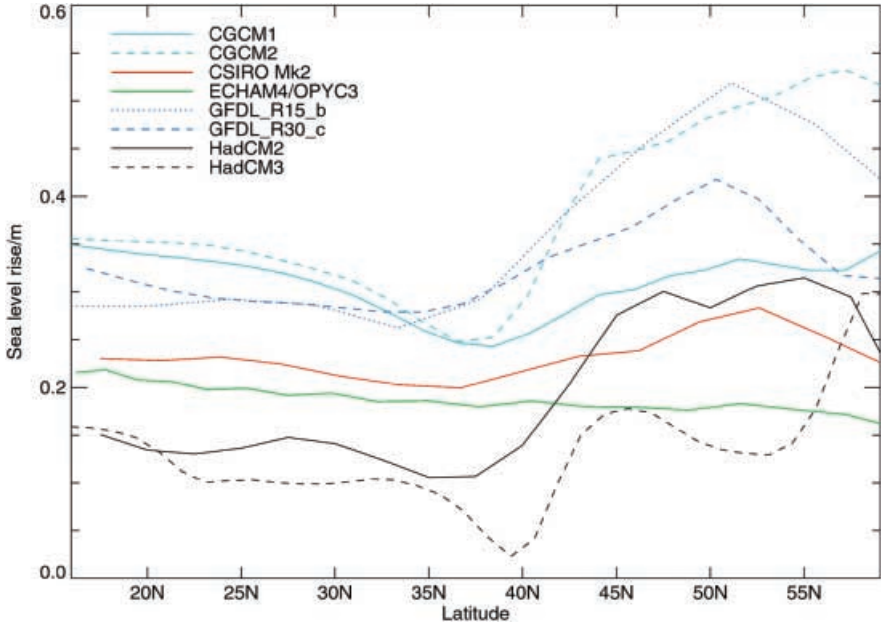

Fig. 6 Sea-level change averaged over 2050–2100 with respect to the control climate as a function of latitude for longitudes 40–50°W

Church et al. (2001) for a discussion. Land movements are not included in the AOGCMs, and are subtracted from tide gauge records before the latter are used to make comparisons with estimates of ocean contributions to sea-level change.

According to Douglas (1992), a tide-gauge record of at least fifty years is needed to obtain a useful estimate of a local trend. There is only a very small set of gauges that cover a long enough period and are free from land movement or can be reliably corrected for it. With such a small set, it is possible that the geographical variation of sea-level change might not be sufficiently sampled, leading to an underestimate of the spatial variance and a possible bias in the global average.

Douglas (1997) calculates the global-average trend as the mean of nine regions, each being represented by a small number of gauges. He gives the standard error of estimate of the global-average trend as 0.1 mm a^{-1}, which implies a spatial standard deviation of about 0.3 mm a^{-1}, i.e. larger by $\sqrt{9}$, assuming the regions are not correlated. This lies within the range given by the models for σ_M^* (Table 4). As the number of gauges increases, it would not be correct to continue to diminish the standard error of the estimated global-average trend indefinitely, because the temporal variability would become spatially correlated. In the limit of sampling everywhere (practically approached by satellite altimetry), there would still remain some statistical uncertainty in the trend, owing to globally correlated temporal variability.

To investigate quantitatively the effect of sampling on spatial variance, we evaluate twentieth-century trends from the AOGCM results for the nine regions used by Douglas (1997, his Table I), choosing one 5°-gridbox in each case. This small sample tends to underestimate the spatial variance of the whole field of trends (Table 4, compare σ_9 with σ_M), maybe because the extreme trends in the models are not adjacent to coasts, where the tide gauges are located. The underestimate is severe in the case of ECHAM4/OPYC3, whose strongest spatial variations occur in the Southern Ocean, a region not sampled at all by tide gauges. The average of the nine gridboxes is fairly near to the global-average trend in most cases; it does not appear to be biased. It should be noted that there may be coastal effects on sea-level change not simulated by any of the models because of their relatively low resolution. For instance, the models could not simulate propagation of signals by coastally trapped waves, in the manner suggested by Hsieh and Bryan (1996).

The small sample size that can be used in practice will also make it harder to detect any acceleration in twentieth-century sea-level rise. Using again the sets of nine gridboxes corresponding to the regions of Douglas (1997), we have also calculated the acceleration from the AOGCM results. Although all the models have a positive acceleration in the average of the nine gridboxes, the acceleration is not statistically distinguishable from zero in most cases, unlike the results based on the complete ocean area (Table 2). If the model variability is realistic, this result suggests that the absence of acceleration in the observations is not necessarily inconsistent with the model predictions of an increasing rate of thermal expansion during the twentieth century.

6 Conclusions

It is expected that the major contribution to sea-level rise over the next hundred years will be thermal expansion, which can be evaluated from AOGCMs. This work compares the results from several AOGCMs for global-average sea-level rise due to thermal expansion in the twentieth and twenty first centuries, and the geographical distribution of sea-level change due to ocean density and circulation changes.

We find that a small network of widely spaced tide gauges, such as that use by Douglas (1997), may somewhat underestimate the spatial variance of local sea-level trends in the twentieth century. In most AOGCMs, the majority of this variance comes from an underlying non-uniformity in the effect of climate change on sea-level, but local temporal variability also makes an important contribution.

The AOGCM estimates of thermal expansion in recent decades (0.6–1.0 mm a^{-1} for 1955–1995) are somewhat larger than estimates based on observations of interior ocean temperature changes. The AOGCMs indicate an increase during the twentieth century in the rate of global-average sea-level rise due to thermal expansion, but the small set of tide gauges with long records would be probably unable to detect an acceleration of the magnitude simulated by the models.

In the twenty first century, the experiments we have used all followed the IS92a scenario. In all the models there is a constant acceleration in global-average sea-level rise due the thermal expansion during the century. They all project a larger average rate for the twenty first century than the twentieth, but their results cover rather a broad range (2.0–3.7 mm a^{-1} for 1990–2090). This range reflects systematic uncertainty in modelling of climate change and of ocean heat uptake.

The pattern of local sea-level change is strongly non-uniform, with some regions experiencing more than twice the global average. In most regions, sea-level changes are significant compared with variability. However, the models show few common features in the geographical distribution of sea-level change, the main exceptions being that nearly all models show more than average sea-level rise in the Arctic Ocean and less than average in the Southern Ocean. The lack of agreement implies that we can have little confidence in regional projections.

Since sea-level change can have important impacts, it is clearly important to be able to make global and regional predictions of it. As we have demonstrated, the models show substantial differences in these quantities. To understand both the similarities and the differences

among models, and thereby to reduce the systematic uncertainty in projections, we conclude there is a need for more detailed analysis and comparisons of the mechanisms which determine the changes in ocean circulation, interior properties and consequent sea-level change.

Appendix

Methods for calculating local sea-level change in rigid-lid models

The way in which sea-level enters the equations of motion of the real ocean is through its effect on the hydrostatic pressure

$$p(z) = \int_z^\eta \rho g \, \mathrm{d}z' \ ,$$

where g is the acceleration due to gravity and η is the local sea-level. Geographical variation in η is of order 1 m. Both z and η are taken as relative to some time-independent surface of constant gravitational potential, to which the sea-surface would be parallel if the ocean were in a steady state of rest. As a consequence of the replacement of varying η with a fixed surface at $z = 0$, the hydrostatic pressure p at level z and geographical location $\mathbf{x}$ in a rigid-lid model has two terms

$$p(\mathbf{x}, z) = p_\rho(\mathbf{x}, z) + p_s(\mathbf{x}) \ ,$$

where

$$p_\rho = \int_z^0 \rho(\mathbf{x}, z') g \, \mathrm{d}z'$$

is the pressure due the weight of water between level z and the lid. The rigid-lid pressure p_s can be converted to sea-surface height according to

$$p_s = \eta \rho_* g \ ,$$

ρ_* being the density of sea-water at the surface. The hydrostatic pressure appears in the equations of motion only as its horizontal gradient $\nabla_H p$. Hence the dynamics of the model determine p_s only to within an arbitrary additive constant. This means that the relative topography of the ocean surface can be obtained, but its absolute height with respect to a frame referred to the solid earth is not known. Despite this, we can work out the local sea-level difference $h(\mathbf{x})$ between one climate state (state 1) and another (state 2) according to

$$h(\mathbf{x}) = \tilde{\eta}_2(\mathbf{x}) - \tilde{\eta}_1(\mathbf{x}) + r \ ,$$

where $\tilde{\eta}_i$ is the relative topography in state i, the arbitrary offsets having been chosen to give a global-average of zero for $\tilde{\eta}$ in each state. The global average of h is thus the separately determined r. This two-part procedure is discussed and justified by Greatbach (1994). To carry out the calculation, three different methods have been used, which we proceed to describe.

Diagnosed $\nabla_H p_s$

The equation of motion of the rigid-lid model can be summarised as

$$\frac{\partial \mathbf{u}_H}{\partial t} = \mathbf{F} - \frac{1}{\rho_0} \nabla_H p_s \ , \tag{4}$$

where $\mathbf{u}_H$ is the horizontal velocity and ρ_0 a nominal density (following the Boussinesq approximation). Here $\mathbf{F}$ represents the acceleration caused by all forces except the rigid-lid pressure gradient $\nabla_H p_s$. These forces are the remainder $\nabla_H p_\rho$ of the pressure gradient, the Coriolis force, and the effects of viscosity and advection.

Integrating this equation vertically gives

$$\int_{-H}^0 \frac{\partial \mathbf{u}_H}{\partial t} \mathrm{d}z = \int_{-H}^0 \mathbf{F} \, \mathrm{d}z - \frac{H}{\rho_0} \nabla_H p_s \ . \tag{5}$$

Because of the rigid lid, volume is conserved, so the vertically integrated velocity has no divergence. Hence taking the divergence of Eq. 5 yields

$$\frac{1}{\rho_0} \nabla_H \cdot (H \nabla_H p_s) = \nabla_H \cdot \int_{-H}^0 \mathbf{F} \, \mathrm{d}z \ . \tag{6}$$

For GFDL_R15_b and GFDL_R30_c, the right-hand side of the elliptic Equation 6 is diagnosed from the model, and the equation is solved for p_s by successive over-relaxation using gradient boundary conditions, as discussed by Pinardi et al. (1995).

Alternatively, we can take the vertical average of Eq. 4:

$$\frac{1}{H} \int_{-H}^0 \frac{\partial \mathrm{u}_H}{\partial t} \mathrm{d}z = \frac{1}{H} \int_{-H}^0 \mathbf{F} \, \mathrm{d}z - \frac{1}{\rho_0} \nabla_H p_s \ .$$

Since the vertically integrated flow is non-divergent, it can be represented by a stream function ψ, leading to

$$\frac{1}{\rho_0} \nabla_H p_s = \frac{1}{H} \int_{-H}^0 \mathbf{F} \, \mathrm{d}z - \frac{1}{H} \mathbf{k} \times \nabla_H \frac{\partial \psi}{\partial t} \ ,$$

where $\mathbf{k}$ is a vertical unit vector. For HadCM2 and HadCM3 (Gregory and Lowe 2000), the relative topography is calculated from this equation by diagnosing the terms on the right-hand side from the model, calculating $\nabla_H p_s$, and extracting p_s by a numerical minimisation.

These two methods both use information from the full equation of motion to obtain p_s up to an additive constant, and hence $\tilde{\eta}$. Any differences between them result only from the numerics of the equation-solvers. The HadCM2/HadCM3 method was also used by Gregory (1993) for an earlier version of the Hadley Centre model, but in that case $\nabla_H p_s$ was not available as a model diagnostic, and had to be estimated from the other terms in the equations of motion. Since geostrophy is a good approximation away from continental boundaries and well below the wind-driven Ekman layer, $\nabla_H p_\rho$ and the Coriolis force were the dominant terms in these estimates.

Geostrophy

For the other rigid-lid models used, geostrophy was assumed in order to compute the relative topography. With the assumption of geostrophy, $\mathbf{F}$ contains only the pressure gradient and the Coriolis force, and acceleration is neglected. The equation of motion is

$$\begin{aligned} \mathbf{0} &= -f \rho_0 \mathbf{k} \times \mathbf{u}_H - \nabla_H p \\ &= -f \rho_0 \mathbf{k} \times \mathbf{u}_H - \nabla_H p_\rho - \nabla_H p_s \ , \end{aligned} \tag{7}$$

where f is the Coriolis parameter. The model velocity field at level z gives us the Coriolis term, and the density field above z the p_ρ term; hence we obtain $\nabla_H p_s$ and extract p_s as before. Alternatively, using the first form of the right-hand side, we obtain $\nabla_H p$, extract p, and then calculate $p_s = p - p_\rho$. The latter underlies the procedure used for the CSIRO Mk2 model, as described by Jackett et al. (2000). The local sea-level change is given by

$$h = \Delta\tilde{\eta} + r = \frac{\Delta p_s}{\rho_0 g} + r = \frac{\Delta p - \Delta p_\rho}{\rho_0 g} + r \ .$$

Jackett et al. (2000) obtain Δp from the inversion of $\nabla_H \Delta p$ and set the arbitrary constant so that Δp, rather than Δp_s, has an area-average of zero. Let us write Δp so adjusted as $\Delta\tilde{p}$. To retain an area-average of zero for Δp_s, the area-average of Δp_ρ must also be subtracted:

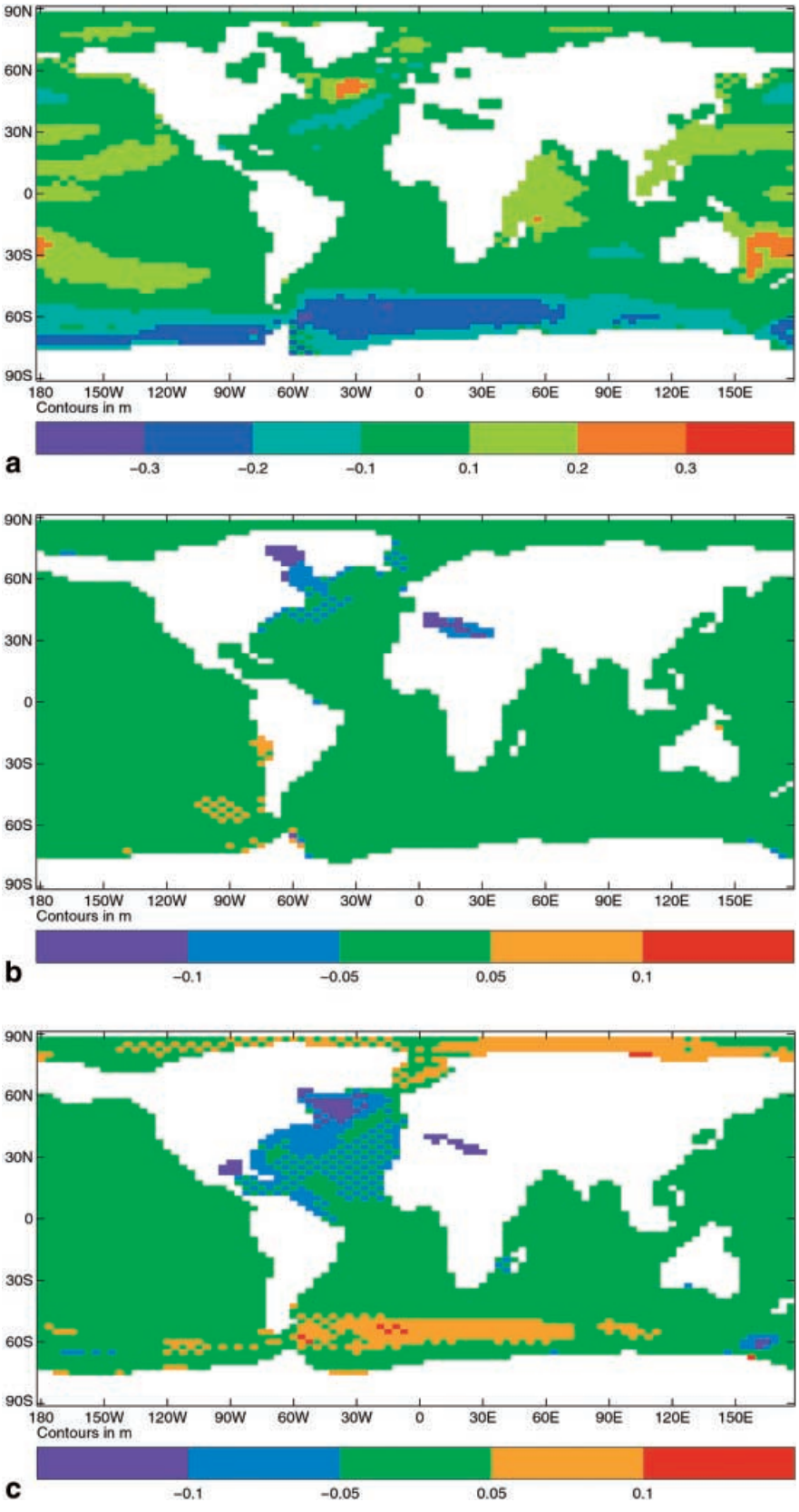

Fig. 7a–c Comparison of different methods of calculating local sea-level change, tested on HadCM2 results. **a** Sea-level change calculated using the diagnosed $\mathbf{V}_H p_s$. **b** Difference from **a** of the result of the method of Jackett et al. (2000), assuming geostrophy. **c** Difference from **a** of the results of the method of dynamic topography, assuming geostrophy and a level of no motion at 1190 m

Table 7 Comparison of results from different methods for calculating the same field of sea-level change

Method	SD/m	Maximum/m	Minimum/m	Correlation
Diagnosed $\mathbf{V}_H p_s$ (Gregory and Lowe 2000)	0.10	0.27	−0.39	1.00
Geostrophy (Jackett et al. 2000)	0.11	0.26	−0.35	0.97
Geostrophy and no motion at 1190 m (Bryan 1996)	0.10	0.28	−0.32	0.94

These three methods were all used to calculate the field of sea-level change shown in Fig. 7a. The statistics here were computed after subtracting the area-weighted average in each case. SD is the area-weighted standard deviation; the correlation is with the results of the first method

$$h = \frac{\Delta\tilde{p} - \Delta\tilde{p}_\rho}{\rho_0 g} + r = \frac{\Delta\tilde{p} - \Delta p_\rho}{\rho_0 g} + r + \frac{1}{\rho_0 g}\frac{1}{S}\int_S \Delta p_\rho \, \mathrm{d}S \ .$$

The two last terms can then be combined as

$$r_z = -\frac{1}{S}\int_S \int_{-H}^{0} \frac{\Delta\rho}{\rho_0}\mathrm{d}z' \, \mathrm{d}S + \frac{1}{\rho_0 g}\frac{1}{S}\int_S \int_z^0 \Delta\rho g \, \mathrm{d}z' \, \mathrm{d}S$$

$$= -\frac{1}{S}\int_S \int_{-H}^{z} \frac{\Delta\rho}{\rho_0}\mathrm{d}z'\mathrm{d}S \ ,$$

i.e. the sea-level rise due to thermal expansion between the bottom of the ocean and level z. Since no value can be computed at points where the ocean is shallower than z, it is best to choose the smallest z which is deep enough to avoid the influence of the wind. Jackett et al. (2000) demonstrate that the method is insensitive to the choice of z, as it should be.

Figure 7a is the local sea-level change in a particular decade of a HadCM2 experiment computed by the method normally employed for HadCM2 results, using the diagnosed $\mathbf{V}_H p_s$; in Fig. 7b we show the difference between this and the same field calculated by the method of Jackett et al. (2000). The difference is less than 0.05 m nearly everywhere and shows no structure other than a small systematic difference between the Pacific and the other oceans. The area-weighted correlation between the fields is high and their statistics are similar (Table 7).

Geostrophy and a level of no motion

The traditional oceanographic method of calculating local sea-level is as the dynamic topography, which in addition to geostrophy assumes a level of no motion i.e. a surface of constant $z = z_0$ on which $\mathbf{u}_H = \mathbf{0}$. This assumption should be reasonably good if z_0 is deep in the interior of the ocean, but not near the bottom. On $z = z_0$, the equation of motion (Eq. 7) simplifies to

$$\mathbf{V}_H p = \mathbf{V}_H p_\rho + \mathbf{V}_H p_s = \mathbf{0} \ ,$$

which is immediately solved by $p_s = -p_\rho + \text{constant}$; unlike in the previous methods, there is no need to extract a scalar from a gradient field. This is how local sea-level was calculated by Bryan (1996). This method cannot give a value for waters shallower than the level of no motion.

Figure 7c exhibits the difference between the results of this method assuming $z_0 = 1190$ m and the $\mathbf{V}_H p_s$ method. The difference has some structures which are related to ocean circulation; the largest discrepancies are of order 0.1 m and occur in regions where there are substantial currents at depth, in the Antarctic Circumpolar Current and North Atlantic. In these regions, the assumption of no motion is probably unsatisfactory, but in general, agreement is almost as good as for the method of Jackett et al. (2000).

Acknowledgements We are grateful to Josef Oberhuber for supplying the data from ECHAM4/OPYC3 and to Badal Pal for his help with computing the CCCma sea-level results. Trevor McDougall, Tony Hirst, two GFDL reviewers and two Climate Dynamics reviewers made helpful comments. Richard Wood and Ulrich Cubasch collected the information about the AOGCMs shown in Table 1; more comprehensive tables of AOGCMs and experiments appear in chapters 8 and 9 of the IPCC WGI Third Assessment Report. Work at the Hadley Centre was supported by the UK Department of the Environment, Transport and the Regions under contract PECD 7/12/37 and the Public Meteorological Service Research and Development Programme. J. A. Church and D. R. Jackett were supported by CSIRO's Climate Change Research Program and were funded in part by Australia's National Greenhouse Research Program.

References

Boer GJ, Flato G, Ramsden D (2000a) A transient climate change simulation with greenhouse gases and aerosol forcing: projected climate to the twenty-first century. Clim Dyn 16(6): 427–450

Boer GJ, Flato G, Reader MC, Ramsden D (2000b) A transient climate change simulation with greenhouse gas and aerosol forcing: experimental design and comparison with the instrumental record for the twentieth century. Clim Dyn 16(6): 405–425

Bryan K (1996) The steric component of sea level rise associated with enhanced greenhouse warming: a model study. Clim Dyn 12: 545–555

Church JA, Gregory JM, Huybrechts P, Kuhn M, Lambeck K, Nhuan MT, Qin D, Woodworth PL (2001) Changes in sea level. In: Houghton JT, Ding Y, Griggs DJ, Noguer M, van der Linden P, Dai X, Maskell K, Johnson CI (eds) Climate change 2001: the scientific basis. Contribution of Working Group I to the Third Assessment Report of the Intergovernmental Panel on Climate Change. Cambridge University Press, Cambridge, UK (in press)

Cubasch U, Santer BD, Hellbach A, Hegerl G, Höck H, Maier-Reimer E, Mikolajewicz U, Stössel A, Voss R (1994) Monte-Carlo climate change forecasts with a global coupled ocean-atmosphere model. Clim Dyn 10: 1–19

Cubasch U, Meehl GA, Boer GJ, Stouffer RJ, Dix M, Noda A, Senior CA, Raper SCB, Yap KS (2001) Projections of future climate change. In: Houghton JT, Ding Y, Griggs DJ, Noguer M, van der Linden P, Dai X, Maskell K, Johnson CI (eds) Climate change 2001: the scientific basis. Contribution of Working Group I to the Third Assessment Report of the Intergovernmental Panel on Climate Change. Cambridge University Press, Cambridge, UK (in press)

De Wolde JR, Huybrechts P, Oerlemans J, van de Wal RSW (1997) Projections of global mean sea level rise calculated with a 2D energy-balance climate model and dynamic ice sheet models. Tellus 49A: 486–502

Dixon KW, Lanzante JR (1999) Global mean surface air temperature and North Atlantic overturning in a suite of coupled GCM climate change experiments. Geophy Res Lett 26: 1885–1888

Douglas BC (1992) Global sea level acceleration. J Geophys Res 97: 12 699–12 706

Douglas BC (1997) Global sea level rise: a redetermination. Surv Geophys 18: 279–292

Ducet N, Le Traon PY, Gauzelin P (1999) Response of the Black Sea mean level to atmospheric pressure and wind forcing. J Mar Syst 22: 311–327

Flato GM, Boer GJ (2001) Warming asymmetry in climate change experiments. Geophys Res Lett 28: 195–198
Flato GM, Boer GJ, Lee WG, McFarlane NA, Ramsden D, Reader MC, Weaver AJ (2000) The Canadian Climate Centre for Climate Modeling and Analysis global coupled model and its climate. Clim Dyn 16(6): 451–467
Gordon HB, O'Farrell SP (1997) Transient climate change in the CSIRO coupled model with dynamic sea ice. Mon Weather Rev 125: 875–907
Gordon C, Cooper C, Senior CA, Banks H, Gregory JM, Johns TC, Mitchell JFB, Wood RA (2000) The simulation of SST, sea ice extents and ocean heat transports in a version of the Hadley Centre coupled model without flux adjustments. Clim Dyn 16: 147–168
Gornitz V, Rosenzweig C, Hillel D (1997) Effects of anthropogenic intervention in the land hydrological cycle on global sea level rise. Global Planet Change 14: 147–161
Greatbach RJ (1994) A note on the representation of steric sea level in models that conserve volume rather than mass. J Geophys Res 99: 12 767–12 771
Gregory JM (1993) Sea level changes under increasing atmospheric CO_2 in a transient coupled ocean–atmosphere GCM experiment. J Climate 6: 2247–2262
Gregory JM (2000) Vertical heat transports in the ocean and their effect on time-dependent climate change. Clim Dyn 16: 501–515
Gregory JM, Mitchell JFB (1997) The climate response to CO_2 of the Hadley Centre coupled AOGCM with and without flux adjustment. Geophys Res Lett 24: 1943–1946
Gregory JM, Lowe JA (2000) Predictions of global and regional sea-level rise using AOGCMs with and without flux adjustment. Geophys Res Lett 27: 3069–3072
Hasselmann K, Sausen R, Maier-Reimer E, Voss R (1993) On the cold start problem in transient simulations with coupled atmosphere-ocean models. Clim Dyn 9: 53–61
Haywood JM, Stouffer RJ, Wetherald RT, Manabe S, Ramaswamy V (1997) Transient response of a coupled model to estimated changes in greenhouse gas and sulfate concentrations. Geophys Res Lett 24: 1335–1338
Hirst AC, Gordon HB, O'Farrell SP (1996) Global warming in a coupled climate model including oceanic eddy-induced advection. Geophys Res Lett 23: 3361–3364
Hirst AC, O'Farrell SP, Gordon HB (2000) Comparison of a coupled ocean-atmosphere model with and without oceanic eddy-induced advection. Part I. Ocean spinup and control integrations. J Clim 13: 139–163
Hsieh WW, Bryan K (1996) Redistribution of sea level rise associated with enhanced greenhouse warming: a simple model study. Clim Dyn 12: 535–544
Jackett DR, McDougall TJ, England MH, Hirst AC (2000) Thermal expansion in ocean and coupled general circulation models. J Clim 13: 1384–1405
Johns TC, Carnell RE, Crossley JF, Gregory JM, Mitchell JFB, Senior CA, Tett SFB, Wood RA (1997) The second Hadley Centre coupled ocean-atmosphere GCM: model description, spinup and validation. Clim Dyn 13: 103–134
Johns TC, Gregory JM, Ingram WJ, Johnson CE, Jones A, Lowe JA, Mitchell JFB, Roberts DL, Sexton DMH, Stevenson DS, Tett SFB, Woodage MJ (2001) Anthropogenic climate change for 1860 to 2100 simulated with the HadCM3 model under updated emissions scenarios. HCTN 22, Hadley Centre
Keen AB, Murphy JM (1997) Influence of natural variability and the cold start problem on the simulated transient response to increasing CO_2. Clim Dyn 13: 847–864
Knutti R, Stocker TF (2000) Influence of the thermohaline circulation on projected sea level rise. J Clim 13: 1997–2001
Latif M, Roeckner E, Mikolajewicz U, Voss R (2000) Tropical stabilisation of the thermohaline circulation in a greenhouse warming simulation. J Clim 13: 1809–1813
Leggett J, Pepper WJ, Swart RJ (1992) Emissions scenarios for the IPCC: an update. In: Houghton JT, Callander BA, Varney SK (eds) Climate change 1992: the supplementary report to the IPCC scientific assessment: Cambridge University Press, Cambridge, UK pp 69–96
Levitus S, Antonov JI, Boyer TP, Stephens C (2000) Warming of the world ocean. Science 287: 2225–2229
Manabe S, Stouffer RJ (1994) Multiple century response of a coupled ocean-atmosphere model to an increase of atmospheric carbon dioxide. J Clim 7: 5–23
Manabe S, Stouffer RJ, Spelman MJ, Bryan K (1991) Transient responses of a coupled ocean-atmosphere model to gradual changes of atmospheric CO_2. Part I: annual mean response. J Clim 4(8): 785–818
Meier MF (1984) Contribution of small glaciers to global sea level. Science 226: 1418–1421
Miller JR, Russell GL (2000) Projected impact of climate change on the freshwater and salt budgets of the Arctic Ocean by a global climate model. Geophys Res Lett 27: 1183–1186
Mitchell JFB, Johns TC, Gregory JM, Tett SFB (1995) Climate response to increasing levels of greenhouse gases and sulphate aerosols. Nature 376: 501–504
Mitchell JFB, Johns TC, Ingram WJ, Lowe JA (2000) The effect of stabilising atmospheric carbon dioxide concentrations on global and regional climate change. Geophys Res Lett 27: 2977–2980
Mitchell JFB, Karoly DJ, Hegerl GC, Zwiers FW, Allen MR, Marengo J (2001) Detection of climate change and attribution of causes. In: Houghton JT, Ding Y, Griggs DJ, Noguer M, van der Linden P, Dai X, Maskell K, Johnson CI (eds) Climate change 2001: the scientific basis. Contribution of Working Group I to the Third Assessment Report of the Intergovernmental Panel on Climate Change. Cambridge University Press, Cambridge, UK (in press)
Mitrovica JX, Tamisiea ME, Davis JL, Milne GA (2001) Recent mass balance of polar ice sheets inferred from patterns of global sea-level change. Nature 409: 1026–1029
Murphy JM, Mitchell JFB (1995) Transient response of the Hadley Centre coupled ocean-atmosphere model to increasing carbon dioxide. Part II: spatial and temporal structure of response. J Clim 8: 57–80
Nakiboglu SM, Lambeck K (1991) Secular sea-level change. In: Sabadini R, Lambeck K, and Boschi E (eds) Glacial isostasy, sea level and mantle rheology. Kluwer, Dordrecht, pp 237–258
Pinardi N, Rosati A, Pacanowski RC (1995) The sea surface pressure formulation of rigid lid models. Implications for altimetric data assimilation studies. J Mar Sys 6: 109–119
Ponte RM, Gaspar P (1999) Regional analysis of the inverted barometer effect over the global ocean using TOPEX/POSEIDON data and model results. J Geophys Res 104: 15 587–15 601
Raper SCB, Gregory JM, Osborn TJ (2001) Use of an upwelling-diffusion energy balance climate model to simulate and diagnose A/OGCM results. Clim Dyn 17: 601–613
Roeckner E, Oberhuber JM, Bacher A, Christoph M, Kirchner I (1996) ENSO variability and atmospheric response in a global coupled atmosphere-ocean GCM. Clim Dyn 12: 737–754
Roeckner E, Bengtsson L, Feichter J, Lelieveld J, Rodhe H (1999) Transient climate change simulations with a coupled atmosphere–ocean GCM including the tropospheric sulfur cycle. J Clim 12(10): 3004–3032
Russell GL, Gornitz V, Miller JR (2000a) Regional sea-level changes projected by the NASA/GISS atmosphere-ocean model. Clim Dyn 16: 789–797
Russell GL, Miller JR, Rind D, Ruedy RA, Schmidt GA, Sheth S (2000b) Comparison of model and observed regional temperature changes during the past 40 years. J Geophys Res 105: 14 891–14 898
Sahagian D (2000) Global physical effects of anthropogenic hydrological alterations: sea level and water redistribution. Global Planet Change 25: 39–48
Stouffer RJ, Manabe S (1999) Response of a coupled ocean–atmosphere model to increasing atmospheric carbon dioxide: sensitivity to the rate of increase. J Clim 12: 2224–2237
Trupin A, Wahr J (1990) Spectroscopic analysis of global tide gauge sea level data. Geophys J Intern 100: 441–453

Voss R, Mikolajewicz U (2001) Long-term climate changes due to increased CO_2 concentration in the coupled atmosphere-ocean general circulation model ECHAM3/LSG. Clim Dyn 17: 45–60

Warrick RA, Le Provost C, Meier MF, Oerlemans J, Woodworth PL (1996) Changes in sea level. In: Houghton JT, Filho LGM, Callander BA, Harris N, Kattenberg A, Maskell K (eds) Climate change 1995. The science of climate change. Cambridge University Press, Cambridge, UK, pp 359–406

Weaver AJ, Wiebe EC (1999) On the sensitivity of projected oceanic thermal expansion to the parameterisation of sub-grid scale ocean mixing. Geophys Res Lett 26: 3461–3464

Wigley TML, Raper SCB (1993) Future changes in global mean temperature and sea level. In: Warrick RA, Barrow EM, Wigley TML (eds) Climate and sea level change: observations, projections, and implications. Cambridge University Press, Cambridge, UK, pp 113–133

Wigley TML, Raper SCB (1995) An heuristic model for sea level rise due to the melting of small glaciers. Geophys Res Lett 22: 2749–2752

Zuo Z, Oerlemans J (1997) Contribution of glacier melt to sea level rise since AD 1865: a regionally differentiated calculation. Clim Dyn 13: 835–845